Comparative analysis of the temperature dependences of the resistivity, pseudogap, and thermoelectric power in polycrystals YBa$_2$Cu$_3$O$_{7-\delta}$ with a decrease in the density of charge carriers

A. L. Solovjov, V. B. Stepanov, and Yu. A. Kolesnichenko

B. Verkin Institute for Low Temperature Physics and Engineering of the National Academy of Sciences of Ukraine
Kharkiv 61103, Ukraine
E-mail: solovjov@ilt.kharkov.ua

Comparative analysis of the temperature dependences of resistivity $\rho(T)$, excess conductivity $\sigma'(T)$, pseudogap (PG) $\Delta^*(T)$, and thermoelectric power $S(T)$, measured on textured YBa$_2$Cu$_3$O$_{7-\delta}$ (YBCO) polycrystals with different charge carrier density n_f, depending on the level of doping with oxygen, modified by annealing, has been carried out. It is shown that for an optimally doped (OD) sample with $T_c = 90$ K (sample S1), $\sigma'(T)$ near T_c is well described by the Aslamazov–Larkin (AL-3D) and Maki–Thompson (MT-2D) fluctuation theories, demonstrating 3D–2D crossover with increasing temperature. The crossover temperature T_0 was used to determine the coherence length along the c axis, $\xi_c(0)$. With a decrease in n_f (samples S2 with $T_c = 84$ K and S3 with $T_c = 80$ K), the MT contribution is suppressed, and the $\sigma'(T)$ dependence obeys the Lawrence–Doniach model, which is typical for samples with defects. The dependence $\Delta^*(T)$ obtained for S1 has a form typical for OD single crystals of YBCO with a maximum at $T_{pair} \sim 114$ K and a linear section descending to $T_{01} \sim 94$ K, which limits the region of superconducting fluctuations above T_c. As n_f decreases, the shape of $\Delta^*(T)$ noticeably changes and becomes typical for YBCO films with a symmetric maximum at T_{pair}, which is the BEC–BCS transition temperature in high-T_c superconductors. As n_f decreases, the slope $S(T)$ changes from positive to negative, demonstrating a feature at the PG opening temperature T^*. Accordingly, the dependence of $S(T)/T$ on log T changes from linear to nonlinear, which indicates a change in the nature of interactions in the YBCO electronic subsystem with decreasing n_f, since $S/T \sim 1/n_f$.

Keywords: high-temperature superconductivity, fluctuation conductivity, thermoEMF, YBCO polycrystals.

1. Introduction

The study of the mechanism of superconducting (SC) pairing in high-temperature superconductors (HTSCs), which still remains unclear, is still one of the central directions of research in condensed matter physics. Understanding the mechanism of SC pairing is extremely important for the search for HTSCs with even higher, preferably room, critical temperatures, T_c, for the transition to the SC state. It is believed that the study of the so-called pseudogap state [1–3], which is observed in the region of the phase diagram corresponding to the appropriate concentration of charge carriers less than optimal, which is usually called the region of "underdoped" states, can shed light on this, as well as a number of other issues. Pseudogap (PG) is a special state of matter, which is characterized by a reduced (but not to zero) density of electronic states (DOS) at the Fermi level [4, 5]. It should be emphasized that the pseudogap state is fundamentally different from the superconducting one, in which the SC gap opens and DOS is zero [6]. In HTSC cuprates of the YBa$_2$Cu$_3$O$_{7-\delta}$ (YBCO) type, the pseudogap opens at the characteristic temperature $T^* \gg T_c$. As a result, in a wide temperature range below T^*, HTSCs have a number of unusual properties due to, as it is now commonly believed, the rearrangement of the Fermi surface [7–9]. However, the physical reason for the occurrence of the PG state is also not completely clear and continues to be the subject of extensive discussions [10–14].

There are two main groups of models for explaining the PG in cuprates. The first is based on the idea that PG is a

precursor to superconductivity and arises as a result of the formation of paired fermions, the so-called local pairs (LPs) below T^* [3, 7, 15–19] with the subsequent establishment of their phase coherence at T_c [20]. Thus, this model states the superconducting nature of the PG. In one version of such model [3, 16, 17], the superconducting transition is considered as a Bose–Einstein condensation (BEC) of gas of electron pairs, considered as bosons with a charge of $2e$. This model works at low-electron concentrations, which exactly corresponds to the PG region in the HTSC cuprates. Unfortunately, the BEC model does not discuss the SC pairing mechanism, which leads to the appearance of such bosons above T_c.

The second group of models assumes that the origin of the PG state is associated, for example, with low-energy antiferromagnetic fluctuations [7, 21, 22], since in the region of low hole concentrations all known HTSC cuprates are antiferromagnetic dielectrics [3, 7, 8]. The charge (CDW) [7, 8] and spin (SDW) [2, 7, 23] density waves, structural distortions [24], as well as recently developed ideas on modulation of the order parameter in HTSC (pair-density wave (PDW) state) [14, 25 (and references therein)], on which there is a strong scattering of electrons, leading to a pseudogap rearrangement of their spectrum, are also not excluded. In such models, the non-superconducting nature of the PG state is stated. Thus, at present, there is still no consensus on the nature of the PG and its relation to superconductivity.

It is well known that all properties of HTSC cuprates are determined by the density of charge carriers n_f, which can vary in a wide range depending on the doping level [3, 7, 26, 27]. In YBCO n_f changes as a result of oxygen intercalation, and the maximum $T_c \sim 91$ K corresponds to the stoichiometric material at $\delta = 0$ [26]. In this paper, we report on the measurement of temperature dependences of the resistivity $\rho(T)$ and the thermoelectric power (TEP) $S(T)$ in three textured polycrystalline YBCO samples with different n_f, which changed as a result of annealing the samples. For brevity, we will refer to the samples as S1, S2, and S3. From measurements of $\rho(T)$, data were extracted on the excess conductivity, $\sigma'(T)$, and, accordingly, on the temperature dependence of the fluctuation conductivity (FLC) and pseudogap, $\Delta^*(T)$. The calculation of the dependences $\Delta^*(T)$ was carried out in the model of local pairs [1, 3, 15–17], and the results were compared with the corresponding dependences $\rho(T)$ and $S(T)$ in order to find a correlation between the various features found in the PG phase in different experiments. As far as we know, the Seebeck coefficient $S(T)$ has not yet been compared with the temperature dependences of resistance and PG.

The results obtained show that in the region of superconducting (SC) fluctuations near T_c, FLC of the optimally doped sample S1 is perfectly described by the classical fluctuation theories of Aslamazov–Larkin (3D-AL) [28] and Hikami–Larkin (HL) (fluctuation contribution of Maki–Thompson

(2D-MT) [29–31], and the shape $\Delta^*(T)$ is the same as in the YBCO films without defects [3, 17]. D is the dimension of the HTSC electronic subsystem. In the S2 and S3 samples, MT contribution is completely suppressed, and $\sigma'(T)$ is described in Lawrence–Doniach model most likely as a result of defects arising during annealing [24]. Simultaneously the shape of $\Delta^*(T)$ and $S(T)$ is also changed. It has been found that regardless of the density of charge carriers, $S(T)$ of all three samples clearly changes the slope at the PG opening temperature T^*. A discussion of these and other results obtained is given below.

2. The experiment

The samples were parallelepipeds with a length of 10 mm and a cross-section of 3 by 2 mm, cut from a pellet of textured polycrystalline $YBa_2Cu_3O_{7-\delta}$ with a diameter of 30 mm and a thickness of 5 mm, obtained by solid-phase synthesis from yttrium and copper oxides and barium carbonate [32]. Initially, the sample had a value of $T_c \sim 90$ K (S1). A decrease in the oxygen content and, consequently, the density of charge carriers n_f, and, therefore, T_c, was achieved by thermal vacuum annealing. Initially, three 90 K samples were prepared. The second was annealed at temperature ~ 350 °C and the third one was annealed at temperature ~ 400 °C, both in an oxygen-free environment for half an hour. After the first annealing $T_c = 84$ K was obtained (sample S2), and eventually the sample S3 with $T_c = 80$ K was prepared.

The electrical resistivity was measured in a wide temperature range from ~ 290 K to T_c utilizing the four-point probe technique with stabilized measuring current of up to 10 mA. Silver epoxy contacts were glued to the extremities of the sample in order to produce a uniform current distribution in the central region where voltage probes were placed. To measure $S(T)$, potential contacts were clamped to the upper surface of the sample and were usually located at a distance of ~ 6 mm from each other. Thermoelectric power measurements were carried out by using the differential method over the same temperature range. A temperature gradient of ~ 1 K was maintained throughout the measurements. A differential thermocouples made from copper and constantan and calibrated with a silicon diode sensor (DT 470) were used to measure the temperature of the test sample, while thermoelectric voltage (ΔV) developed across the sample due to the temperature gradient (ΔT) was measured by a Keithley 2000 Multimeter. The thermoelectric power $S(T)$ calculated from the linear fits of ΔV vs ΔT curve was corrected for copper electrodes to obtain absolute thermoelectric power values [33]. More details of the experimental technique are given elsewhere [34].

A feature of polycrystals is that their n_f can change noticeably upon annealing the sample, both in an oxygen atmosphere (to increase n_f) and without it (to decrease n_f). However, in the case of a strong change in n_f, various kinds of defects can appear in the samples [24], which can

affect the measurements of ρ(*T*) and, to a much lesser extent, *S*(*T*), since the Seebeck coefficient is measured at low currents and is a characteristic of material, and not a specific sample with its defects.

3. Results and discussion

3.1. Resistivity, critical temperature, and thermoelectric power

Figure 1 displays the temperature dependences of the resistivity, ρ(*T*), and the absolute TEP, *S*(*T*), of all three polycrystalline YBa$_2$Cu$_3$O$_{7\delta}$ samples with different oxygen content, and, consequently, with different T_c: S1 — T_c = 90 K, S2 — T_c = 84 K, and S3 — T_c = 80 K. As usual, T_c was determined by extrapolating the linear portion of the ρ(*T*) dependence at SC transition to its intersection with the temperature axis [35], that is, $T_c \equiv T_c$ (ρ$_{ex}$ = 0). In the case of S1, the width of the resistive transition δT_c = T_c(0.9ρ$_N$) − − T_c(0.1 ρ$_N$) ≈ 2.5 K is rather narrow, but increases almost fourfold for sample S3. However, since the linear portion of the ρ(*T*) dependence at the SC transition is well pronounced for all samples, this approach makes it possible to determine the values of T_c with an accuracy of ± 0.1 K (Table 1). All dependences ρ(*T*) exhibit metallic behavior and are linear above T^*: ρ$_N$(*T*) = ρ$_0$ + *aT*, with a slope *a* = = *d*ρ/*dT* ≈ 5.76 μΩcm/K (S1). ρ$_0$ is the residual resistance, which the extrapolated ρ$_N$(*T*) cuts off on the Y axis. The slope was calculated by approximating the experimental curves on a computer and confirmed the linear behavior of ρ(*T*) with a root-mean-square error of 0.023 ± 0.002 in a given temperature range for all samples.

As can be seen from Table 1, the resistivity of the samples during annealing increases markedly. However, with a decrease in T_c from 90 K to 84 K, the slope of ρ(*T*) practically does not change. This fact suggests that in our samples at large n_f, the Matthiessen's rule is fulfilled in a good approximation, namely: ρ = ρ$_0$ + ρ$_{id}$, where ρ$_{id}$ is the
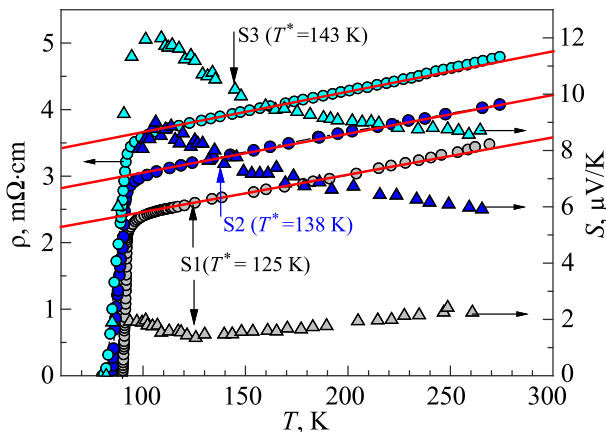

Fig. 1. (Color online) The temperature dependences of resistivity ρ and Seebeck coefficient *S* for YBa$_2$Cu$_3$O$_{7-\delta}$ polycrystals S1 (T_c = 90 K), S2 (T_c = 84 K) and S3 (T_c = 80 K).

Table 1. Changes in the parameters of the YBa$_2$Cu$_3$O$_{7-\delta}$ polycrystal upon annealing

Samples	T_c, K	ρ(300 K), μΩ·cm	ρ(100 K), μΩ·cm	ρ$_0$, μΩ·cm	*d*ρ/*dT*, μΩ·cm/K
S1	90	3540	2350	1874	5.76
S2	84	4230	2950	2513	5.75
S3	80	4940	3550	3053	6.12

resistivity of an ideal crystal [36]. In our case, this is, in fact, the resistivity of an unannealed sample containing a minimum number of defects. It can be seen from the Table 1 that the resistivity of the samples upon annealing actually increases due to an increase in ρ$_0$, which occurs as a result of an increase in the number of defects. In contrast to YBCO single crystals, in which twins and pronounced twin boundaries are present, in good polycrystals such defects can be point defects arising with an increase in the number of oxygen vacancies in the CuO$_2$ planes [37].

With a decrease in T_c to 80 K, the slope still slightly increases to *d*ρ/*dT* = 6.12 μΩ/K (S3). Note that a similar increase in *d*ρ/*dT* is observed both in films [17] and in YBCO single crystals [26] with decreasing n_f. At the same time, the residual resistivity ratio, defined as ρ(300 K)/ρ(100 K), slightly decreases from 1.4 (S1) to 1.27 (S3), which also indicates an increase in the number of defects during annealing.

As expected, sample S1 has the highest T_c = (90.0 ± 0.1) K and the smallest ρ(*T* = 100 K) = 2350 μΩ·cm, as well as the lowest maximum value S_{max} = 1.93 μV/K. In this case, the dependence *S*(*T*) is almost linear with a positive slope, which changes to negative clearly at T^* (Fig. 1). For samples S2 and S3, the resistivity ρ(100 K) is 1.26 and 1.51 times higher, respectively (Table 1). In this case, *S*(*T*) of both samples at high temperatures is also close to linear and, curiously, with almost the same but already negative slope, which increases almost 2 times at $T \leq T^*$. A change in the slope *S*(*T*) with decreasing n_f in YBCO was reported in a number of works [38–40], but the fact that the slope changes precisely at $T = T^*$ was shown for the first time. For a more precise definition of T^*, we use the criterion (ρ(*T*) − ρ$_0$)/*aT* [41]. In the normal state (ρ$_N$(*T*) − ρ$_0$)/*aT* = 1, but deviates downward from unity at $T = T^*$, which makes it possible to obtain T^* values with an accuracy of ± 0.3 K [35, 37, 41]. According to the model of LPs [1, 3, 15–17] at $T = T^*$ part of the normal electrons is transformed into local pairs, which transfer charge without dissipation. We believe that this is precisely what leads to an increase in the slope and to faster growth of *S*(*T*) below T^*. Having reached the maximum, *S*(*T*) begins to decrease rapidly and, together with the resistance, turns to zero also practically in T_c. In Fig. 1, these portions of the *S*(*T*)curves are not shown in order not to overload the figure.

At the first stage, the thermoelectric power data were analyzed within the "Two band model with modified linear *T*-term". This model was originally proposed to describe the temperature dependences of the Seebeck coefficient in $CeNi_x$ compounds [43]. But then it was successfully used for $S(T)$ analysis in HTSC systems [40, 42, 44], taking into account the assumption of a Lorentz resonance near the Fermi level. The following formulas were used to analyze the data:

$$S = \frac{AT}{B^2 + T^2}, \quad A = \frac{2(E_F - E_0)}{e},$$

$$B^2 = 3 \frac{(E_F - E_0)^2 - \Gamma^2}{\pi^2 k_B^2}, \qquad (1)$$

where AT shows the conduction of metallic holes and B/T the conduction of the semiconductor type electrons. E_0 and Γ are the center and width of the resonance, respectively. The theory is based on a localized band in density of states $D(E)$ near the Fermi level, which is superimposed on a broadband [40]. Accordingly, the value $(E_F - E_0)$ determines the position of the Fermi level relative to the middle of the peak $D(E)$ (see Fig. 3(a) in Ref. 40). This resonance peak gives the characteristic temperature dependence of TEP. To explain the temperature dependence of TEP in HTSCs, the linear term αT was added to Eq. (1) for $S(T)$, which represents the contribution of the normal band [40, 44, 45]:

$$S = \frac{AT}{B^2 + T^2} + \alpha T. \qquad (2)$$

Equation (2) has been used to fit TEP data for HTSCs by many research groups, and the results obtained showed good agreement with experimental results, especially well above T_c [40, 45 and references therein)]. However, from Eq. (2), the TEP is expected to become zero at 0 K, but for
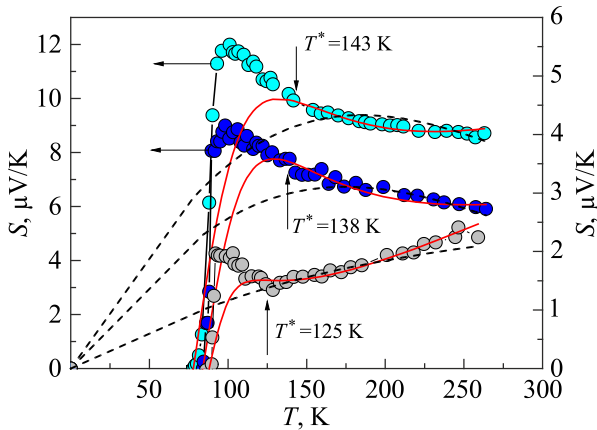

Fig. 2. (Color online) Temperature dependences of *S* for $YBa_2Cu_3O_{7-\delta}$ polycrystals S1 ($T^* = 125$ K), S2 ($T^* = 138$ K), and S3 ($T^* = 143$ K) in comparison with theoretic models (2) (black dashed curves) and (3) (red solid curves).

Table 2. Results of experimental data processing within the framework of the model (3)

Samples	T_c, K	A, μV	B, K	α, $\mu V/K^2$	$E_F - E_0$, meV	Γ, meV	T_{s0}, K
S1	90	52	22	0.0127	0.026	3.43	88
S2	84	570	40.5	0.017	0.285	6.32	84
S3	80	800	46	0.026	0.4	7.17	78

HTSCs, the TEP drops to zero just below T_c. To eliminate this inconsistency, the temperature *T* has been replaced by $(T - T_{s0})$ in Eq. (2) as shown below [45]:

$$S = \frac{A(T - T_{S0})}{B^2 + (T - T_{S0})^2} + \alpha(T - T_{S0}), \qquad (3)$$

where $T_{s0} \approx T_c$ is the temperature of zero TEP for HTSCs.

Temperature dependencies of experimental TEP data for samples S1, S2, and S3 are shown in Fig. 2. The experimental $S(T)$ data were fitted to the formula (3) (red curves) and the fitting parameters are given in Table 2. Let's note the following. Model (3) gives good agreement between the experimental and calculated curves for all samples, and with reasonable values of the parameters. Unlike $Y_{1-x}Pr_xBa_2Cu_3O_y$ [40], with a decrease in the concentration of charge carriers, all parameters are gradually increased. Interestingly, both the width of the resonance peak Γ and the value $(E_F - E_0)$ increase linearly. That is, as well as in $Y_{1-x}Pr_xBa_2Cu_3O_y$ the Fermi level moves to the upper edge of the band [40], suggesting the observed increase in the TEP value [46]. However, it should be noted that the fitting is incomplete. Indeed, all theoretical curves deviate downward from the experiment at $T \leq T^*$. This result seems to be quite reasonable since it is believed that at $T \leq T^*$, the PG opens in the HTSCs and the rearrangement of the Fermi surface begins [5, 7–9].

As a result, the Lorentz resonance near the Fermi level can be suppressed, making the model (3) inapplicable. In addition, the black dashed curves in the figure correspond to model (2) and clearly do not fit the experiment. Therefore, model (2) is not considered in detail. We awaited more information, comparing the $S(T)$ data with the results of the FLC and PG analysis as shown below.

3.2. Fluctuation conductivity

The linear $\rho(T)$ above T^* was proven to be an integral feature of the normal state of cuprates (e.g., YBCO) [47], which is characterized by the stability of the Fermi surface [5, 7–9], as mentioned above. At $T \leq T^*$ the $\rho(T)$ deviates downward from the linearity, resulting in appearance of the excess conductivity $\sigma'(T)$:

$$\sigma'(T) = \sigma(T) - \sigma_N(T) = \frac{1}{\rho(T)} - \frac{1}{\rho_N(T)}, \qquad (4)$$

where $\rho_N(T) = aT + \rho_0$ is the resistivity of the sample in the normal state, extrapolated to the low temperature region. It is worth noting that at $T = T^*$ not only $\rho(T)$ deviates downward from linearity but also DOS at the Fermi level begins to gradually decrease, which means the opening of PG [2, 4, 5]. In addition, at $T = T^*$ the Fermi surface is believed to change [7–9], most likely because of the formation of the LPs just below T^* [3, 15, 16]. Thus the proper determination of T^* is of a primary importance for the FLC and PG analysis. Fortunately, the above precise method for finding T^* allows a quite well way of determining T^* with sufficient accuracy.

In accordance with modern concepts [1, 3, 15, 16, 27, 48–51], the small coherence length in combination with the quasi-layered structure of HTSCs leads to the formation of a noticeable, in comparison with conventional superconductors, range of SC fluctuations, ΔT_{fl}, in cuprates above T_c. In this range, fluctuating Cooper pairs (FCPs) behave in a good many ways like ordinary SC pairs, but without long-range order (the so-called "short-range phase correlations") [1–3, 10–16, 48], and the excess conductivity, $\sigma'(T)$, obeys the classical fluctuation theories [28–31]. Usually, in YBCO, $\Delta T_{fl} = T_{01} - T_G = (10–20)$ K, where T_G is the Ginsburg temperature, down to which the Bogolyubov mean-field theory works. The range of ΔT_{fl} is determined by a change in the oxygen stoichiometry, the presence of impurities and/or structural defects which have a significant effect on $\sigma'(T)$ and, accordingly, on the implementation of various models for describing the FLC above T_c [24, 28–31, 47]. Importantly, as mentioned above the behavior of TEP in the range of SC fluctuations has not yet been studied in detail.

In order to estimate the FLC within the local pair model [1, 3, 15, 16], it is also necessary to determine the critical temperature in the mean-field approximation, T_c^{mf} [3, 51, 52], which limits the range of critical fluctuations around T_c, in which the order parameter $\Delta < k_B T$ [52, 53]. The T_c^{mf} is an important parameter of both FLC and PG analysis since it determines the reduced temperature $\varepsilon = \dfrac{T - T_c^{mf}}{T_c^{mf}}$, which is included in all equations. In HTSCs near T_c, the FLC is always described by the Aslamazov–Larkin [28] equation for any 3D systems [3, 35, 51, 54]:

$$\sigma'_{AL3D} = C_{3D} \frac{e^2}{32 h \xi_c(0)} \varepsilon^{-1/2}. \quad (5)$$

To determine T_c^{mf} we use an approach proposed by Beasley, *et al.*: from Eq. 5, $\sigma'^{-2}(T) \sim \varepsilon \sim T - T_c^{mf}$ and is zero when $T = T_c^{mf}$ [52]. The result is shown in Fig. 3, using S1 as an example. Also shown are T_c, the Ginsburg temperature $T_G > T_c^{mf}$, and 3D–2D crossover temperature T_0. Using the same approach, T_c^{mf} for all samples was obtained (Table 1). Having determined both T^*, $\sigma'(T)$ and T_c^{mf}, we can plot the
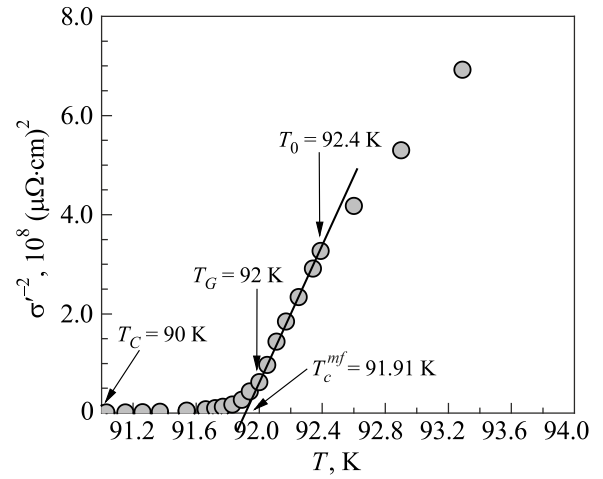

Fig. 3. Temperature dependence of the inverse square of the excess conductivity, $\sigma'^{-2}(T)$, for the polycrystal of $YBa_2Cu_3O_{7-\delta}$ with $T_c = 90$ K (sample S1), which determines $T_c^{mf} = 91.9$ K. The arrows also show T_c, the Ginzburg temperature T_G, and the 3D–2D crossover temperature T_0.

dependences $\ln\sigma'$ versus $\ln\varepsilon$ for each sample. Figure 4 shows results for S1 (a) and S3 (b). As in all cuprates [24, 54], near T_c, $\ln\sigma'$ in both S1 and S3 is well described by Eq. (5). In the figure, these are straight red lines (1) with a slope $\lambda = -1/2$. This is because at $T < T_0$ the coherence length along the c axis, $\xi_c(T) = \xi_c(0)\varepsilon^{-1/2} > d = 11.67$ Å, which is the YBCO unit cell size along the c axis [55], and FCPs can interact in the entire sample volume forming the 3D state. It should be noted that S1 demonstrates the behavior of FLC, which is characteristic of well-structured YBCO, both films [53] and single crystals [54]. Indeed, above the 3D–2D crossover temperature T_0 (marked as $\ln \varepsilon_0 = -5.25$ in the figure) the data deviates above the 3D–AL line and can be well described by the 2D Maki–Thompson (2D–MT) equation of the Hikami–Larkin theory [29]:

$$\sigma'_{MT} = C_{2D} \frac{e^2}{8 d \hbar} \cdot \frac{1}{1 - \alpha/\delta} \cdot \ln\left((\delta/\alpha) \cdot \frac{1 + \alpha + \sqrt{1 + 2\alpha}}{1 + \delta + \sqrt{1 + 2\delta}} \right), \quad (6)$$

where $\alpha = 2[\xi_c(0)/d]^2 \varepsilon^{-1}$ is the coupling parameter,

$$\delta = \beta \frac{16}{\pi \hbar} \left[\frac{\xi_c(0)}{d} \right]^2 k_B T \tau_\varphi \quad (7)$$

is the pair-breaking parameter, $\tau_\phi \beta T = \pi h / 8 k_B \varepsilon_0 = A / \varepsilon_0$ is the lifetime of the FCPs and $A = 2.998 \cdot 10^{-12}$ sK. The factor $\beta = 1.203(\ell / \xi_{ab})$, where ℓ is the mean free path and $\xi_{ab}(T)$ is the coherence length in the ab plane, corresponds to the case of the clean limit $(\ell > \xi)$ [3, 29, 31]. On a double logarithmic scale Eq. (6) is the solid blue curve in Fig. 4(a), which perfectly describes the data in the range between T_{01} $(\ln\varepsilon_{01} = -3.45$ in the figure) and T_0. This is because at $T_0 < T < T_{01}$ $d > \xi_c(T) > d_{01} \approx 4$ Å [55], which is the distance between the conducting CuO_2 planes. Thus the planes
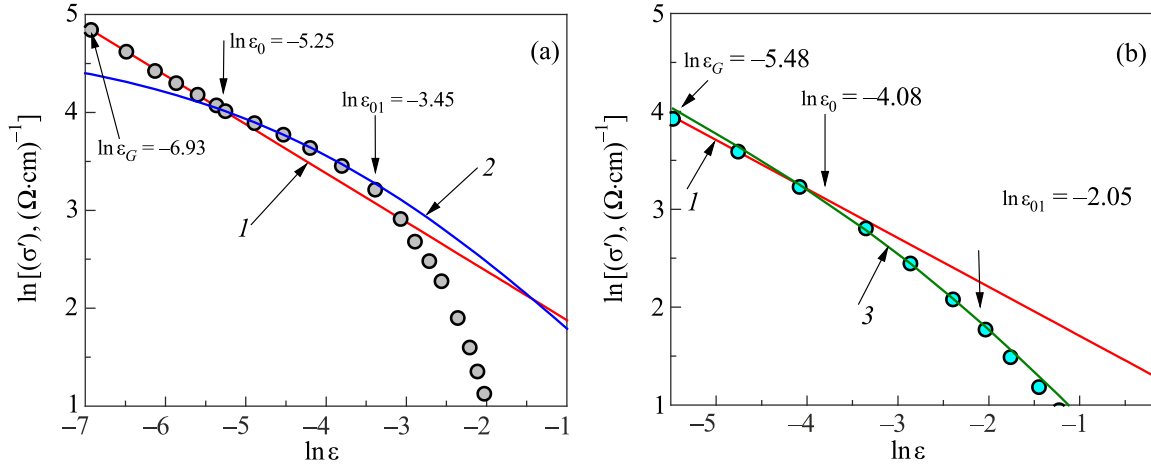
Fig. 4. (Color online) $\ln\sigma'$ vs $\ln\varepsilon$ of the $YBa_2Cu_3O_{6.94}$ polycrystal with T_c = 90 K [S1, gray dots, (a)] and after annealing to the T_c = 80 K [S3, green dots, (b)] in comparison with fluctuation theories: 3D-AL (red solid lines *1*), 2D-MT [blue solid curve *2*, (a)], and LD [green solid curve *3*, (b)]. $\ln(\varepsilon_G)$ determines the Ginzburg temperature T_G, $\ln(\varepsilon_0)$ determines the crossover temperature T_0, and $\ln(\varepsilon_{01})$ determines T_{01}, which limits the region of the SC fluctuations from above.

are connected by the Josephson interaction forming the 2D fluctuating state of cuprates [29, 30]. Accordingly, at $T = T_0$ $\xi_c(T_0) = d$ [3, 35, 53, 54]. This allows the determination of the coherence length along the c axis [51, 54]

$$\xi_c(0) = d\sqrt{\varepsilon_0} . \qquad (8)$$

Taking found $T_0 \approx 92.4$ K ($\ln\varepsilon_0 \approx -5.25$) into account, from the Eq. (8) we find $\xi_c(0) = (0.86 \pm 0.02)$ Å (S1), which is a typical value of $\xi_c(0)$ for optimally doped untwined YBCO single crystals with close T_c = 91.6 K [54]. In turn, S3 demonstrates the behavior of FLC, which is characteristic of YBCO films with defects [52] and indicates the formation of point defects in the sample upon annealing, as mentioned above [37]. Indeed, above $T_0 \approx 92$ K (denoted in the figure as $\ln\varepsilon_0 = -4.08$), the data deviate downward from the 3D–AL line [Fig. 4(b)] and can be well described by the Lawrence–Doniach (LD) [56] equation of the Hikami–Larkin theory [29]:

$$\sigma'_{LD} = C_{LD}\frac{e^2}{16\hbar d\sqrt{1+2\alpha}}\varepsilon^{-1}. \qquad (9)$$

In this equation, we note that σ' will diverge as $\varepsilon^{-1/2}$ (3D behavior) when the temperature is close to T_c^{mf}, and that σ' will go as ε^{-1} dependence (2D behavior) at sufficiently

high temperature such that $2\xi_c(T)/d <1$. On a double logarithmic scale, this is the solid green curve in Fig. 4(b), which perfectly describes the data in the range between $T_{01} \approx 102$ K ($\ln\varepsilon_{01} = -2.05$ in the figure) and T_0. Taking found T_0 into account, from the Eq. (8) we find $\xi_c(0) = (1.52 \pm 0.02)$ Å (S3), which, as expected, increased with decreasing T_c in accordance with the theory of superconductivity [6]. Above T_{01} the CuO_2 planes are no longer related by the correlation interaction [27, 30], since now $\xi_c(T) < d_{01}$, the experimental data completely deviate down from the theory. It is clear that $\xi_c(T_{01}) = d_{01}$ and finally $d_{01} = d\sqrt{\varepsilon_0/\varepsilon_{01}} = (4.5 \pm 0.3)$ Å [3, 35, 53, 54], which is close to the inter-planar distance in YBCO [55]. Found from the FLC analysis $\xi_c(0)$ are important parameters for calculating the temperature dependences of PG, as will be shown below.

3.3. Analysis of the pseudogap temperature dependence

To analyze the excess conductivity $\sigma'(T)$ in the entire temperature range from T^* down to T_G we use equation [17]

$$\sigma'(T) = A_4\frac{e^2(1-T/T^*)\exp(-\Delta^*/T)}{16\hbar\xi_c(0)\sqrt{2\varepsilon_{c0}^*}\sinh(2\varepsilon/\varepsilon_{c0}^*)}, \qquad (10)$$

where $(1 - T/T^*)$ determines the number of pairs arising at $T \le T^*$, and $\exp(-\Delta^*/T)$ gives the number of pairs destroyed by thermal fluctuations below T_{pair} [3, 17]. The equation (10) is based on ideas from Leridon, *et al.* [57] but markedly modified to provide the best fit for $\sigma'(T)$ over the entire temperature range from T^* down to T_G. In addition, it was successfully used to describe the excess conductivity in different HTSCs [3, 17, 24, 35, 54, 58] including FeAs-based superconductors [59]. Solving Eq. (10) with respect to $\Delta^*(T)$, we obtain the equation for the PG [17]:

Table 3. Parameters of the FLC analysis of $YBa_2Cu_3O_{7-\delta}$ polycrystal at different annealing

Samples	T_c^{mf}, K	T_G, K	T_{01}, K	$\xi_c(0)$, Å	d_{01}, Å
S1	91.91	92.0	94.8	0.86	4.82
S2	90.62	90.7	99.7	1.4	4.41
S3	90.8	90.8	102.5	1.52	4.24

$$\Delta^*(T) =$$

$$= T \ln \left[A_4 \left(1 - \frac{T}{T^*} \right) \frac{1}{\sigma'(\varepsilon)} \frac{e^2}{16 \hbar \xi_c(0)} \frac{1}{\sqrt{2\varepsilon_{c0}^*} \sinh(2\varepsilon / \varepsilon_{c0}^*)} \right],$$

(11)

where $\sigma'(T)$ is the experimentally determined excess conductivity.

In addition to T^*, T_c^{mf}, ε, and $\xi_c(0)$, which were already defined above, both equations contain $\Delta^*(T_G)$, the theoretical parameter ε_{c0}^* [57] and the coefficient A_4, which has the same meaning as the C-factor in the theory of FLC [30]. It is believed, that in cuprates $\Delta^*(T_G) = \Delta(0)$, which is a SC energy gap at $T = 0$ [17, 60, 61]. Thus, $\Delta^*(T_G)$ determines the actual PG value in the sample. Note that in the model of LPs, all parameters included in Eqs. (10) and (11) can be directly determined from experiment [3, 17, 24, 35, 54], as discussed below.

To find $\Delta^*(T_G)$, we plot the experimental values of excess conductivity in coordinates $\ln\sigma'$ vs $1/T$ [3, 17] (Fig. 5) and approximate them by the theoretical dependences $\ln\sigma'(1/T)$ calculated by the Eq. (10) (red curve in Fig. 5). With this construction, the shape of the theoretical curve turns out to be very sensitive to the value of $\Delta^*(T_G)$ [17, 24, 35]. The best approximation is achieved at the value of the Bardeen–Cooper–Schrieffer (BCS) ratio $D^* = 2\Delta(0)/k_B T_c = 2\Delta^*(T_G)/k_B T_c = 5.2$ for S1. $D^* = (5\pm0.2)$ is a typical value for YBCO, suggesting the strong coupling limit for HTSCs [62]. To find the theoretical parameter ε_{c0}^* [57] we use the experimental fact that in the region $\ln\varepsilon_{c01} < \ln\varepsilon < \ln\varepsilon_{c02}$ (refer to Fig. 6) $\sigma'^{-1} \sim \exp(\varepsilon)$ [17, 24, 54]. As a result, in the temperature range $\varepsilon_{c01} < \varepsilon < \varepsilon_{c02}$, $\ln(\sigma'^{-1})$ is a linear function of ε with a slope $\alpha^* = 17$, which defines the parameter $\varepsilon_{c0}^* = 1/\alpha^* \approx 0.059$ for S1 (refer to inset to Fig. 6). Now the coefficient A_4 can be determined. For this, using Eq. (10), the dependence
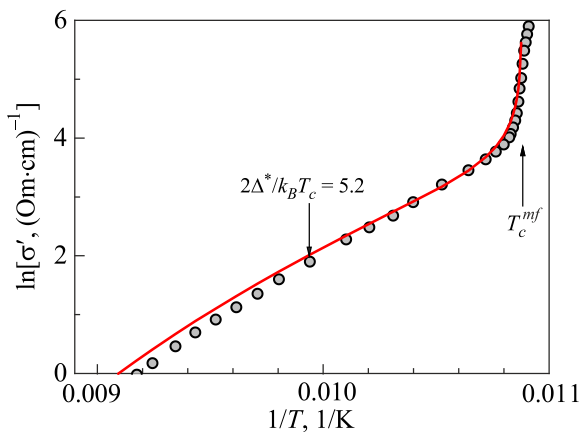

Fig. 5. (Color online) $\ln\sigma'$ as a function of $1/T$ of the sample S1 in the entire temperature range from T^* down to T_c^{mf} (gray dots). Red curve is approximation of experimental data by Eq. (10) with a set of parameters given in the text. The best approximation is achieved at the value of the BCS ratio $D^* = 2\Delta^*(T_G)/k_B T_c = 5.2$.
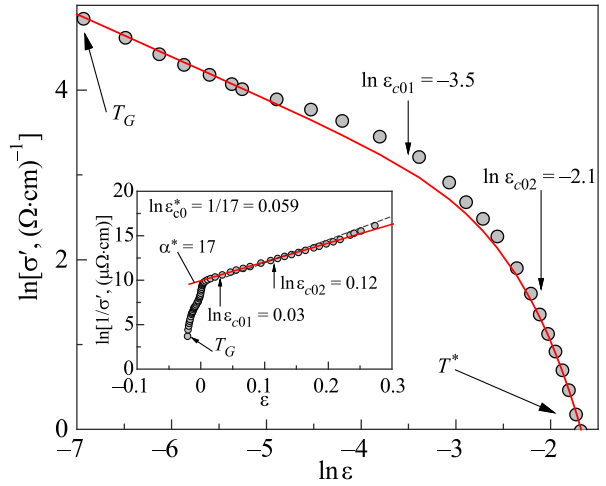

Fig. 6. (Color online) $\ln\sigma'$ as a function of $\ln\varepsilon$ (dots) of the sample S1 in the entire temperature range from T^* down to T_G. Red curve is approximation of experimental data by Eq. (10) with a set of parameters given in the text. Insert: $\ln(1/\sigma')$ as a function of ε. The red straight line denotes the linear part of the curve between $\varepsilon_{c01} = 0.03$ and $\varepsilon_{c02} = 0.12$. The corresponding values of $\ln(\varepsilon_{c01})$ and $\ln(\varepsilon_{c02})$ are indicated by arrows on the main panel. The slope $\alpha^* = 17$ determines the parameter $\varepsilon_{c0}^* = 1/\alpha^* \approx 0.059$ [57].

$\sigma'(T)$ is calculated with the parameters already found and, selecting A_4, is combined with the experiment in the region of 3D–AL fluctuations, where $\ln\sigma'$ is a linear function of $\ln\varepsilon$ with the slope $\lambda = -1/2$ [29, 30, 49, 52] (Fig. 6, red curve). The fit gives $A_4 = 0.22$ for S1. For all the samples under study, the similar graphs were obtained as in Figs. (5), (6), and the corresponding parameters were found for samples S2 and S3 (Table 4).

Having determined all necessary parameters (refer to Tables 1, 2, and 3) we were able to plot the temperature dependences PG, $\Delta^*(T)$, for all samples. For example, the curve $\Delta^*(T)$ for S1 is calculated using Eq. (11) with the following set of parameters: $T^* = 125$ K, $T_c^{mf} = 91.91$ K, $\xi_c(0) = 0.86$ Å, $\varepsilon_{c0}^* = 0.059$, and $A_4 = 0.22$. The corresponding parameters determined for S2 and S3 are listed in the tables. The results are shown in Fig. 7(a)–(c) together with $\rho(T)$ and $S(T)$. S1 demonstrates $\Delta^*(T)$ [Fig. 7(a)], which is typical for optimally doped (OD) single crystals with a moderate number of defects and very likely without twins [63]. The pseudogap $\Delta^*(T)$ sharply increases in the range $T^* > T > T_{pair}$ demonstrating maximum at $T_{pair} \sim 114$ K, which is characteristic of OD YBCO single crystals [64]. Recall that T_{pair} corresponds to the temperature at which LPs transform from strongly bound bosons SBBs into FCPs [3, 17]. As in OD YBCO single crystals, below T_{pair}, the $\Delta^*(T)$ dependence becomes linear with a positive slope down to T_{01} (red line in the figure). In addition, $\Delta^*(T)$ shows a minimum at $T = T_{01}$, a maximum at about T_0, and a final small minimum at T_G. This behavior of $\Delta^*(T)$ near T_c is typical for all well structured HTSCs [35, 54, 63], including even FeSe [65].

Table 4. Parameters of the pseudogap analysis of YBa$_2$Cu$_3$O$_{7-\delta}$ at different annealing

Samples	T^*, K	T_{pair}, K	ε^*_{c0}	A_4	D^*, K	$\Delta^*(T_{pair})$, K	$\Delta^*(T_G)$, K	S_{max}, µV/K
S1	125	114	0.06	0.22	5.2	245	236	1.93
S2	138	100	0.09	0.33	5.4	237	226	9.0
S3	143	107	0.22	0.17	5.0	239	200	12

Upon annealing, not only T_c changes, but the shape of the dependences $\Delta^*(T)$ also changes noticeably [Figs. 7(b) and (c)]. Ultimately, at $T_c = 80$ K, the shape of the $\Delta^*(T)$ becomes the same as in well-structured YBCO films [17] and single crystals [54], with a wide maximum at T_{pair}. Indeed, the more defects, the more isotropic the sample [37]. However, the behavior of $\Delta^*(T)$ near T_c is noticeably violated, namely: the minimum at T_{01} and the maximum at T_0 disappear, but the minimum remains at T_G. Most likely, this is a feature of polycrystals with defects, which leads to very low values of T_{pair} observed in the experiment. As can be seen from Table 4, the values of D^* and $\Delta^*(T_{pair})$ remains almost independent on the charge carrier density n_f. At the same time, as expected, the "fundamental" value of $\Delta^*(t) = \Delta(0)$ [60, 61] noticeably decreases upon annealing, that is, with a decrease in n_f. This result seems reasonable, since a decrease in T_G with decreasing n_f is clearly observed for both YBCO [17] and BiSCCO (Bi-2212) cuprates [66]. In Fig. 7, in addition to $\Delta^*(T)$, are also shown $\rho(T)$ and $S(T)$ for each specimen S1, S2, and S3, allowing details of the behavior of PG and TEP to be analyzed.

Above T^*, $S(T)$ is perfectly approximated by the model (3), as noted above (red curves at the bottom of Fig. 7). At $T \leq T^*$ the slope of the $S(T)$ curves markedly changes. Comparison with $\Delta^*(T)$ convincingly shows that the growth of $S(T)$ begins precisely at T^*. It is currently believed that the opening of PG in cuprates at T^* is accompanied by a rearrangement of the Fermi surface [7–9, 67] due to the formation of bound fermions, the so-called LPs [10–16]. As a result, model (3) does not fit the $S(T)$ data below T^*. However, since the resistivity decreases below T^*, it can be concluded that LPs can transfer electric charge without dissipation [16], which can lead to the observed increase in $S(T)$. Interestingly, with a decrease in the density of charge carriers n_f upon annealing, $S(T)$ increases by more than 6 times (Table 4). Figure 7 also shows that TEP of all three samples reaches maximum at T_{01}, then begins to decrease in the region of SC fluctuations, and, as expected, rapidly drops to zero below T_G. The fact that the TEP demonstrates a maximum precisely at $T = T_{01}$ was also discovered for the first time.
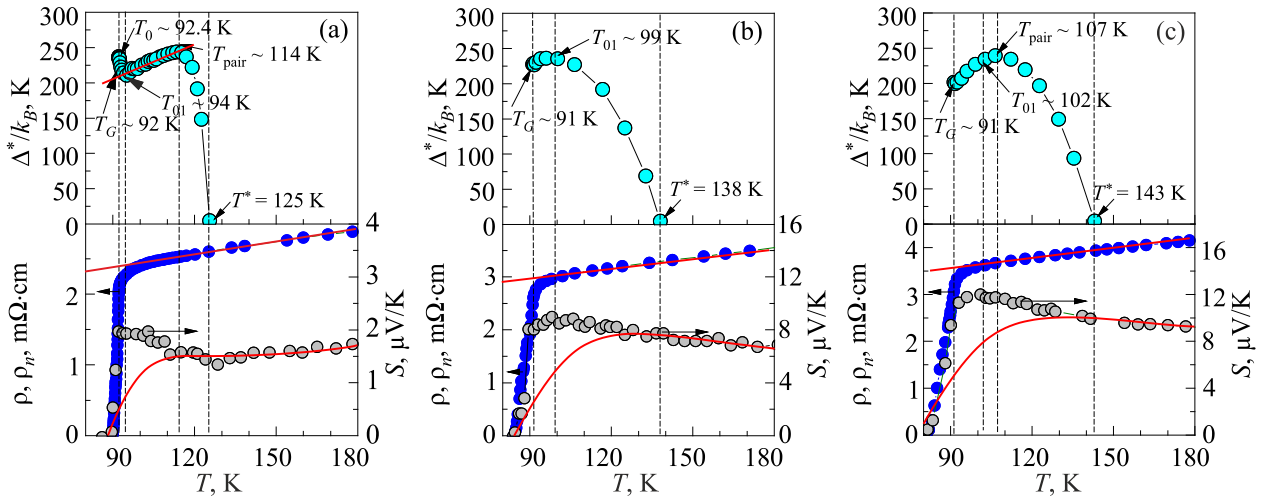

Fig. 7. (Color online) (a) Upper panel: the temperature dependence of the pseudogap $\Delta^*(T)$ for sample S1 (dots) calculated using Eq. (11) with the set of parameters given in the text. The red line denotes the linear part of $\Delta^*(T)$ below T_{pair}. Arrows indicate the corresponding characteristic temperatures. Solid curve is guidance for eye. Bottom panel: $\rho(T)$ (blue dots) and $S(T)$ (gray dots) for S1. Red line denotes $\rho_N(T)$ extrapolated to low T. Red curve is a fit of the $S(T)$ data by the model (3). (b) Upper panel: the temperature dependence of the pseudogap $\Delta^*(T)$ for sample S2 (dots) calculated using Eq. (11) with the set of parameters given in the text. Arrows indicate the corresponding characteristic temperatures. Solid curve is guidance for eye. Bottom panel: $\rho(T)$ (blue dots) and $S(T)$ (gray dots) for S2. Red line denotes $\rho_N(T)$ extrapolated to low T. Red curve is a fit of the $S(T)$ data by the model (3). (c) Everything is the same for sample S3.

3.4. Analysis of the thermopower dependence on charge carrier density

Unfortunately, there is no consensus on the mechanism that governs the thermoelectric power in cuprates. While phonon drag has been invoked to explain the temperature dependence in $Bi_2Sr_2CaCu_2O_{8+x}$ (Bi-2212) [68], it is not satisfactory for the case of YBCO where neither electron-phonon nor mass-enhancement mechanisms are adequate [69, 70]. It is believed that both the temperature and doping dependence of S are of electronic origin at least below 100 K [67]. It has been shown theoretically that in the limit of dominant impurity scattering, $S/T \sim (C_e/T)(1/n_f e)$, where C_e is the electronic specific heat, n_f is the density of charge carriers, and e is the charge of the electron [71] for a wide range of strongly correlated electron systems [72]. Therefore, at low temperature the thermoelectric power approximately represents the electronic heat capacity per charge carrier [67]. To elucidate the evolution of TEP and clarify the possible change of electron interaction in our samples with decreasing n_f upon annealing, we analyzed the S/T vs log T curves within the framework of the model developed. The results are shown in Fig. 8. As can be seen from the figure, three different types of S/T vs log T behavior are observed.

Recall that the line marking the approximate position of the pseudogap temperature T^* on the YBCO phase diagram falls to zero at $p^* = 0.19 \pm 0.01$, which corresponds to critical doping, below which, as is known, a PG appears, i.e., so-called quantum critical point [7, 8]. At the same time, at $H = 0$, the T^* line intersects the SC dome approximately at $p^* = 0.16$ [8], which corresponds to the OD YBCO system, roughly to our sample S1 ($T_c = 90$ K). As a result, in this case S/T, exhibits a perfect log $(1/T)$ dependence from ~ 280 K down to T_G, with the expected change of the slope at T^* (Fig. 8). For sample S2 with doping less than p^* ($T_c = 84$ K), S/T is nonlinear at high T, but becomes linear below T^* (Fig. 8). That is, the expected
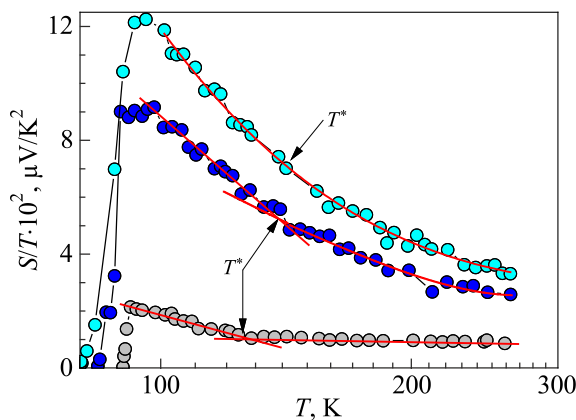
dependence $\log(1/T)$ is observed in a wide temperature range at $T < T^*$. This result is in good agreement with the dependence of S/T on log $(1/T)$ obtained in [67] for $La_{1.6-x}Nd_{0.4}Sr_xCuO_4$ (Nd-LSCO) with p relatively close to p^*. For sample S3 with doping much less than p^* ($T_c = 80$ K), S/T is nonlinear, in the whole temperature range of interest, from ~ 280 K down to T_G, and undergoes a large increase at low temperature. This result is in good agreement with the dependence of S/T on $\log(1/T)$ obtained in [67] for Nd-LSCO with $p < p^*$. The observed similarity with the results obtained at Nd-LSCO suggests that there are three different regimes of quantum criticality in both materials: relatively flat in the Fermi liquid state, which we probably observe for S1, logarithmically divergent at the critical point $p = p^*$ and a jump in the ordered state, which are typical signs of a quantum phase transition in HTSCs at $p \leq p^*$. According to Ref. 67 we can conclude that these observations suggest that p^* is a quantum critical point, below which some order sets in, causing the reconstruction of the Fermi surface, the fluctuations of which are presumably responsible for the logarithmic thermoelectric power. We also believe that the possibility of observing such behavior of TEP in our samples is most likely associated with a rather high degree of impurity scattering in YBCO polycrystals due to the presence of defects, taken into account in the theory [71].

4. Conclusion

For the first time, a comparative analysis of the temperature dependences of resistivity $\rho(T)$, fluctuation conductivity $\sigma'(T)$, pseudogap $\Delta^*(T)$ and thermoelectric power $S(T)$, measured on optimally doped textured $YBa_2Cu_3O_{7-\delta}$ (YBCO) polycrystals before and after annealing, has been carried out. Annealing was performed in two stages, which led to a noticeable decrease in T_c from 90 K (sample S1) to 84 K (S2) and, finally, to 80 K (S3), most likely due to a decrease in the charge carrier density n_f. The resistance of the samples in the course of annealing noticeably increases, but the slope $d\rho/T$ in the region of linear behavior of $\rho(T)$ above T^* practically does not change. This suggests that, in our samples at large n_f, Matthiessen's rule is satisfied in a good approximation. That is, the resistance of the sample during annealing actually increases due to an increase in ρ_0, which occurs as a result of an increase in the number of point defects in the sample. This conclusion is supported by the results of the FLC analysis. In the case of S1, $\ln \sigma'$ vs $\ln \varepsilon$ demonstrates a clear contribution of 2D–MT fluctuations above the 3D–2D crossover temperature T_0, which is typical of well-structured HTSCs [Fig. 4(a)]. After annealing (sample S3), the MT term is completely suppressed, and $\ln \sigma'$ vs $\ln \varepsilon$ above T_0 is described by the LD model typical of HTSCs with defects [Fig. 4(b)].

In contrast to the resistivity, the temperature dependence of the PG, $\Delta^*(T)$, turned out to be more informative (Fig. 7). S1 demonstrates $\Delta^*(T)$ [Fig. 7(a)], which is typical

Fig. 8. (Color online) S/T as a function of log T for samples S1 (gray dots, $T^* = 125$ K), S2 (blue dots, $T^* = 138$ K), and S3 (green dots, $T^* = 143$ K). All solid lines and curves are eye guidance.

for optimally doped single crystals with a moderate number of defects and without twins [63]. It is shown that $\Delta^*(T)$ sharply increases in the range $T^* > T > T_{pair}$ demonstrating maximum at $T_{pair} \sim 114$ K, which is characteristic of OD YBCO single crystals [64]. Below T_{pair}, the $\Delta^*(T)$ dependence becomes linear with a positive slope down to T_{01} (red line in the figure). In addition, $\Delta^*(T)$ shows a minimum at $T = T_{01}$, a maximum at about T_0, and a final small minimum at T_G. This behavior of $\Delta^*(T)$ near T_c is typical for all HTSCs [35, 54, 63], including even FeSe [65]. Upon annealing the dependences $\Delta^*(T)$ change noticeably [Figs. 7(b), and 7(c)]. Ultimately, at $T_c = 80$ K, the shape of the $\Delta^*(T)$ becomes the same as in well-structured YBCO films [17] and single crystals [54], with a wide maximum at T_{pair}. Indeed, the more defects, the more isotropic the sample [37]. However, the behavior of $\Delta^*(T)$ near T_c is noticeably violated, namely: the minimum at T_{01} and the maximum at T_0 disappear, but the minimum remains at T_G. Most likely, this is a feature of polycrystals with defects, which leads to very low values of T_{pair} observed in the experiment. But the values of D^* and $\Delta^*(T_{pair})$ remains almost independent on the charge carrier density n_f (Table 4), while, as expected, the "fundamental" value of $\Delta^*(T_G) = \Delta(0)$ [60, 61] noticeably decreases upon annealing, i.e., with decreasing of n_f. This result seems reasonable since a decrease in $\Delta^*(T_G)$ is clearly observed for both YBCO [17] and BiSCCO (Bi-2212) cuprates [66] with decreasing in n_f. However, due to the lack of a rigorous PG theory, it is impossible to draw an unambiguous conclusion from these results about the change in the electronic interactions in the sample.

Somewhat unexpectedly, it turned out that the study of TEP provides more relevant information. The $S(T)$ analysis was carried out in two stages. We first tried to describe $S(T)$ in terms of the "Two band model with modified linear T-term" which is based on the fact that the TEP in HTSCs is similar to heavy fermion systems with mixed-valence [42, 43]. The results shown in Figs. 2 and 7 by red curves describe the data well, but only above T^*, making it impossible to obtain information about the change of interaction in the electronic subsystem in the pseudogap state. Then we examined the $S(T)$ data within the approach proposed in Ref. 67.

Unfortunately, there is still no consensus on the mechanism that governs the thermoelectric power in cuprates. However, it is believed that both the temperature and doping dependence of S are of electronic origin at least below 100 K [67]. It has been shown theoretically that in the limit of dominant impurity scattering, $S/T \sim (C_e/T)(1/n_f e)$, where C_e, is the electronic specific heat, n_f is the density of charge carriers, and e is the charge of the electron [71] for a wide range of strongly correlated electron systems. To elucidate the possible change of electron interaction in our samples with decreasing n_f upon annealing, we analyzed the S/T vs $\log T$ within this theory using the approach developed in Ref. 67. Three different types of dependences of

S/T on $\log T$ were observed (Fig. 8), which suggests that the mechanism of electronic interaction in YBCO changes upon annealing, since $S/T \sim 1/n_f$.

It is shown that S1 ($T_c = 90$ K) exhibits rather unusual, almost flat dependence of $\log(1/T)$ from ~ 280 K to T_G, with the expected change in slope at T^*. This dependence is typical for $p \geq p^*$, where reduced charge carrier density p^* corresponds to the quantum critical point in cuprates [8, 67]. Accordingly, S2 ($T_c = 84$ K) exhibits nonlinear S/T at high T, but, as expected, a clear $\log(1/T)$ dependence is observed over a wide temperature range at $T < T^*$. This result is in good agreement with the dependence of S/T on $\log(1/T)$ obtained in [67] for $La_{1.6-x}Nd_{0.4}Sr_xCuO_4$ (Nd-LSCO) with $p \leq p^*$. Ultimately, for sample S3 with doping much less than p^* ($T_c = 80$ K), S/T is nonlinear, in the whole temperature range of interest, from ~ 280 K down to T_G, and undergoes a large increase at low temperature. This result is in good agreement with the dependence of S/T on $\log(1/T)$ obtained in [67] for Nd-LSCO with $p < p^*$. The observed similarity with the results obtained at Nd-LSCO suggests that there are three different regimes of quantum criticality in both materials: relatively flat in the Fermi liquid state, which we probably observe for S1, logarithmically divergent at the critical point $p \leq p^*$ and a jump in the ordered state at $p < p^*$, which are typical signs of a quantum phase transition in HTSCs at $p \leq p^*$. According to Ref. 67 we can conclude that these observations suggest that p^* is a quantum critical point, below which some order sets in, causing the reconstruction of the Fermi surface, the fluctuations of which are presumably responsible for the logarithmic thermoelectric power. The possibility of observing such behavior of TEP in our samples is most likely due to a rather high degree of impurity scattering in YBCO polycrystals due to the presence of grain boundaries, which is assumed in the theory [71].

1. V. M. Loktev, R. M. Quick, and S. G. Sharapov, *Phys. Rep.* **349**, 1 (2001).

2. A. A. Kordyuk, *Fiz. Nizk. Temp.* **41**, 417 (2015) [*Low Temp. Phys.* **41**, 319 (2015)].

3. A. L. Solovjov, *Pseudogap and Local Pairs in high-T_c Superconductors*, Superconductors – Materials, Properties and Applications, A. M. Gabovich (ed.), InTech. Rijeka (2012), Chap. 7, p. 137.

4. H. Alloul, T. Ohno, and P. Mendels, *Phys. Rev. Lett.* **63**, 1700 (1989).

5. Takeshi Kondo, A. D. Palczewski, Y. Hamay, A. D. Palczewski, Y. Hamaya, T. Takeuchi, J. S. Wen, Z. J. Xu, G. Gu, and A. Kaminski, arXiv:1208.3448v1 (2012).

6. P. G. De Gennes, *Superconductivity of Metals and Alloys,* W. A. Benjamin, INC., New York–Amsterdam (1966), p. 280.

7. L. Taillefer, Scattering and pairing in cuprate superconductors, *Annu. Rev. Condens. Matter Phys.* **1**, 51 (2010).

8. S. Badoux, W. Tabis, F. Laliberte, G. Grissonnanche, B. Vignolle, D. Vignolles, J. Beard, D. A. Bonn, W. N. Hardy,

R. Liang, N. Doiron-Leyraud, L. Taillefer, and C. Proust, *Nature (London)* **531**, 210 (2016).

9. Y. Y. Peng, R. Fumagalli, Y. Ding, M. Minola, S. Caprara, D. Betto, M. Bluschke, G. M. De Luca, K. Kummer, E. Lefrançois, M. Salluzzo, H. Suzuki, M. Le Tacon, X. J. Zhou, N. B. Brookes, B. Keimer, L. Braicovich, M. Grilli, and G. Ghiringhelli, *Nat. Mater.* **17**, 697 (2018).

10. V. Mishra, U. Chatterjee, J. C. Campuzano, and M. R. Norman, *Nat. Phys.* **10**, 357 (2014).

11. S. Dzhumanov, E. X. Karimboev, U. T. Kurbanov, O. K. Ganiev, and Sh. S. Djumanov, *Superlattices and Micro-structures* **68**, 6 (2014).

12. S. A. Kivelson, and S. Lederer, *PNAS* **116**, 14395 (2019).

13. N. J. Robinson, P. D. Johnson, T. M. Rice, and A. M. Tsvelik, *Rep. Prog. Phys.* **82**, 126501 (2019).

14. D. Chakraborty, M. Grandadam, M. H. Hamidian, J. C. S. Davis, Y. Sidis, and C. Pépin, *Phys. Rev. B* **100**, 224511 (2019).

15. V. J. Emery and S. A. Kivelson, *Nature* **374**, 434 (1995).

16. M. Randeria, *Nature Phys.* **6**, 561 (2010).

17. A. L. Solovjov and V. M. Dmitriev, *Fiz. Nizk. Temp.* **32**, 139 (2006) [*Low Temp. Phys.* **32**, 99 (2006)].

18. T. Dubouchet, B. Sacepe, J. Seidemann, D. Shahar, M. Sanquer, and C. Chapelier, *Nature Phys.* **15**, 233 (2019).

19. K. Lee, K. Kamiya, M. Nakajima, S. Miyasaka, and S. Tajima, *J. Phys. Soc. Jpn.* **86**, 023701 (2017).

20. T. Timusk and B. Statt, *Rep. Prog. Phys.* **62**, 61 (1999).

21. I. I. Mazin, *Nature (London)* **464**, 183 (2010).

22. A. J. Drew, Ch. Niedermayer, P. J. Baker, F. L. Pratt, S. J. Blundell, T. Lancaster, R. H. Liu, G. Wu, X. H. Chen, I. Watanabe, V. K. Malik, A. Dubroka, M. Rössle, K. W. Kim, C. Baines, and C. Bernhard, *Nat. Mater.* **8**, 310 (2009).

23. G. R. Stewart, *Rev. Mod. Phys.* **83**, 1589 (2011).

24. R. V. Vovk and A. L. Solovjov, *Fiz. Nizk. Temp.* **44**, 111 (2018) [*Low Temp. Phys.* **44**, 81 (2018)].

25. Zengyi Du, Hui Li, Sang Hyun Joo, Elizabeth P. Donoway, Jinho Lee, J. C. Séamus Davis, Genda Gu, Peter D. Johnson, and Kazuhiro Fujita, *Nature* **580**, 65 (2020).

26. Y. Ando, S. Komiya, K. Segawa, S. Ono, and Y. Kurita, *Phys. Rev. Lett.* **93**, 267001 (2004).

27. M. S. Grbic, M. Pozek, D. Paar, V. Hinkov, M. Raichle, D. Haug, B. Keimer, N. Baricic, and A. Dulcic, *Phys. Rev. B* **83**, 144508 (2011).

28. L. G. Aslamazov and A. L. Larkin, *Phys. Lett. A* **26**, 238 (1968); L. G. Aslamazov and A. L. Larkin, *Fizika Tverd. Tela* **10**, 1104 (1968) [in Russian].

29. S. Hikami and A. I. Larkin, *Mod. Phys. Lett. B* **2**, 693 (1988).

30. Y. B. Xie, *Phys. Rev. B* **46**, 13997 (1992)

31. J. B. Bieri, K. Maki, and R. S. Thompson, *Phys. Rev. B* **44**, 4709 (1991).

32. S. I. Bondarenko, V. P. Koverya, A. V. Krevsun, and S. I. Link, *Fiz. Nizk. Temp.* **43**, 1411 (2017) [*Low Temp. Phys.* **43**, 1125 (2017)].

33. V. N. Svetlov, A. L. Solovjov, and V. D. Stepanov, *Fiz. Nizk. Temp.* **38**, 83 (2012) [*Low Temp. Phys.* **38**, 64 (2012)].

34. R. H. Kropschot and F. J. Blatt. *Phys. Rev.* **116**, 617 (1959).

35. A. L. Solovjov, L. V. Omelchenko, V. B. Stepanov, R. V. Vovk, H.-U. Habermeier, H. Lochmajer, P. Przyslupski, and K. Rogacki, *Phys. Rev. B* **94**, 224505 (2016).

36. F. Rullier-Albenque, H. Alloul, and R. Tourbot, *Phys. Rev. Lett.* **91**, 047001 (2003).

37. A. L. Solovjov, L. V. Omelchenko, E. V. Petrenko, G. Ya. Khadzhai, R. V. Vovk, D. M. Sergeyev, and A. Chroneos, *Submitted to Scientific Reports*, (2021).

38. P. J. Ouseph and M. Ray O'Bryan, *Phys. Rev. B* **41**, 4123 (1990).

39. V. E. Gasumyants, V. I. Kaidanov, and E. V. Vladimirskaya, *Physica C* **248**, 255 (1995).

40. O. S. Komarova and V. E. Gasumyants, *Phys. Solid State* **52**, 625 (2010).

41. E. V. L. de Mello, M. T. D. Orlando, J. L. Gonzalez, E. S. Caixeiro, and E. Baggio-Saitovich, *Phys. Rev. B* **66**, 092504 (2002).

42. L. Forro, M. Raki, J. Y. Henry, and C. Ayache, *Solid State Commun.* **69**, 1097 (1989)

43. V. Gottwick, K. Glass, F. Horn, F. Steglich, and N. Greve, *J. Magn. Magn. Mater.* **47**, 536 (1985).

44. L. Forro, J. Lukatela, and B. Keszei, *Solid State Commun.* **73**, 501 (1990).

45. E. Altin, D. M. Gokhfeld, F. Kurt, and Z. D. Yakinci, *J. Mater. Sci: Mater Electron.* **24**, 5075 (2013).

46. A. V. Dmitriev and E. S. Tkacheva, *Moscow University Phys. Bull.* **3**, 38 (2014).

47. B. P. Stojkovic and D. Pines, *Phys. Rev. B* **55**, 8576 (1997).

48. H. Alloul, F. Rullier-Albenque, B. Vignolle, D. Colson, and A. Forget, *EPL* **91**, 37005 (2010).

49. W. Lang, G. Heine, P. Schwab, X. Z. Wang, and D. Bauerle, *Phys. Rev. B* **49**, 4209 (1994).

50. R. V. Vovk, N. R. Vovk, G. Ya. Khadzhai, and O. V. Dobrovolskiy, *Solid State Commun.* **204**, 64 (2015).

51. A. L. Solovjov, E. V. Petrenko, L.V. Omelchenko, R. V. Vovk, I. L. Goulatis, and A. Chroneos, *Sci. Rep.* **9**, 9274 (2019).

52. B. Oh, K. Char, A. D. Kent, M. Naito, M. R. Beasley, T. H. Geballe, R. H. Hammond, A. Kapitulnik, and J. M. Graybeal, *Phys. Rev. B* **37**, 7861 (1988).

53. A. L. Solovjov, H.-U. Habermeier, and T. Haage, *Fiz. Nizk. Temp.* **28**, 24 (2002) [*Low Temp. Phys.* **28**, 17 (2002)].

54. A. L. Solovjov, E. V. Petrenko, L. V. Omelchenko, R. V. Vovk, I. L. Goulatis, and A. Chroneos, *Sci. Rep.* **9**, 9274 (2019).

55. G. D. Chryssikos, *Physica C* **254**, 44 (1995).

56. W. E. Lawrence, and S. Doniach, *Proc. of Twelfth Int. Conf. Low Temp. Phys.*, Kyoto, Japan (1970), E. Kanda (ed.), Keigaku: Tokyo, 361 (1970).

57. B. Leridon, A. Défossez, J. Dumont, J. Lesueur, and J. P. Contour, *Phys. Rev. Lett.* **87**, 197007 (2001).

58. R. V. Vovk, N. R. Vovk, A. V. Samoilov, I. L. Goulatis, and A. Chroneos, *Solid State Commun.* **170**, 6 (2013).

59. A. L. Solovjov, L. V. Omelchenko, A. V. Terekhov, K. Rogacki, R. V. Vovk, E. P. Khlybov, and A. Chroneos, *Mater. Res. Express* **3**, 076001 (2016).

60. J. Stajic, A. Iyengar, K. Levin, B. R. Boyce, and T. R. Lemberger, *Phys. Rev. B* **68**, 024520 (2003).

61. Y. Yamada, K. Anagawa, T. Shibauchi, T. Fujii, T. Watanabe, A. Matsuda, and M. Suzuki, *Phys. Rev. B* **68**, 054533 (2003).

62. K. W. Wang and W. Y. Ching, *Physica C* **416**, 47 (2004).

63. A. L. Solovjov, L. V. Omelchenko, R. V. Vovk, O. V. Dobrovolskiy, S. N. Kamchatnaya, and D. M. Sergeev, *Current Appl. Phys.* **16**, 931 (2016).

64. A. L. Solovjov, L. V. Omelchenko, R. V. Vovk, and S. N. Kamchatnaya, *Fiz. Nizk. Temp.* **43,** 1050 (2017) [*Low Temp. Phys.* **43,** 841 (2017)].

65. A. L. Solovjov, E. V. Petrenko, L. V. Omelchenko, E. Nazarova, K. Buchkov, and K. Rogacki, *Fiz. Nizk. Temp.* **46**, 638 (2020) [*Low Temp. Phys.* **46**, 538 (2020)].

66. Ya. Ponomarev, M. Mikheev, M. Sudakova, S. Tchesnokov, and S. Kuzmichev, *Phys. Status Solidi C* **6**, 2072 (2009).

67. R. Daou, O. Cyr-Choinière, F. Laliberté, D. LeBoeuf, N. Doiron-Leyraud, J.-Q. Yan, J.-S. Zhou, J. B. Goodenough, and Louis Taillefer, *Phys. Rev. B* **79**, 180505(R) (2009).

68. H. J. Trodahl, *Phys. Rev. B* **51**, 6175 (1995).

69. J.-S. Zhou and J. B. Goodenough, *Phys. Rev. B* **51**, 3104 (1995).

70. J. L. Tallon, J. R. Cooper, P. S. I. P. N. de Silva, G. V. M. Williams, and J. W. Loram, *Phys. Rev. Lett.* **75**, 4114 (1995).

71. K. Miyake and H. Kohno, *J. Phys. Soc. Jpn.* **74**, 254 (2005).

72. K. Behnia, D. Jaccard, and J. Flouquet, *J. Phys.: Condens. Matter* **16**, 5187 (2004).

_____

Порівняльний аналіз температурних залежностей питомого опору, псевдощілини та термоЕРС у полікристалах YBa$_2$Cu$_3$O$_{7-\delta}$ при зниженні щільності носіїв заряду

A. L. Solovjov, V.B. Stepanov, Yu. A. Kolesnichenko

Проведено порівняльний аналіз температурних залежностей надлишкової провідності $\sigma'(T)$, псевдощілини (ПЩ) $\Delta^*(T)$ та термоЕРС $S(T)$ в текстурованих полікристалах YBa$_2$Cu$_3$O$_{7-\delta}$ з різною щільністю носіїв заряду n_f в залежності від рівня допування киснем. Показано, що для оптимально допованого (ОД) зразка з $T_c = 90$ K (зразок S1), $\sigma'(T)$ поблизу T_c добре описується флуктуаційними теоріями Асламазова–Ларкіна (АЛ-3D) і Макі–Томпсона (МТ-2D), та демонструє 3D–2D кросовер при підвищенні температури. При температурі кросовера T_0 визначено довжину когерентності вздовж осі c, $\xi_c(0)$. При зменшенні n_f (зразки S2 з $T_c = 84$ K та S3 з $T_c = 80$ K) внесок МТ пригнічується, а залежність $\sigma'(T)$ підпорядковується теорії Лоренца–Доніаха (ЛД), що типово для зразків з дефектами. Отримана для S1 залежність $\Delta^*(T)$ має типовий вигляд для ОД монокристалів YBCO з максимумом при $T_{pair} \sim 114$ K та лінійною ділянкою, що спадає до $T_{01} \sim 94$ K, яка обмежує область надпровідних флуктуацій вище T_c. При зменшенні n_f форма $\Delta^*(T)$ помітно змінюється та стає типовою для плівок YBCO з симетричним максимумом при T_{pair}, яка є температурою БЕК–БКШ переходу у високотемпературних надпровідниках. Зі зменшенням n_f нахил $S(T)$ змінюється від позитивного до від'ємного та демонструє особливість при температурі відкриття ПЩ T^*. Відповідно, залежність $S(T)/T$ від $\log T$ змінюється від лінійної до нелінійної, що вказує на зміну характеру взаємодій в електронній підсистемі YBCO при зменшенні n_f, оскільки $S/T \sim 1/n_f$.

Ключові слова: високотемпературна надпровідність, флуктуаційна провідність, термоЕРС, полікристали YBCO.